Numerical Analysis of Wave-Induced Unsteady Pressure on Ship-Hull Surface

Kyung-Kyu Yang[1]*, Beom-Soo Kim[2], Yonghwan Kim[2], Masashi Kashiwagi[3] and Hidetsugu Iwashita[4]

[1]Dept. of Naval Architecture & Ocean Engineering, Chungnam National University, Daejeon, Korea
[2]Dept. of Naval Architecture & Ocean Engineering, Seoul National University, Seoul, Korea
[3]Dept. of Naval Architecture & Ocean Engineering, Osaka University, Osaka, Japan
[4]Dept. of Transportation and Environmental Systems, Hiroshima University, Higashi-Hiroshima, Japan
E-mail: *kkyang@cnu.ac.kr*

1 INTRODUCTION

An estimation of seakeeping performances is one of the important procedures in safe ship design. Thanks to rapid progress in computing power, many numerical methods, such as potential flow solvers and computational fluid dynamics (CFD), have been applied to estimate a ship's behavior in various environmental conditions. To establish reliable numerical methods for the prediction of ship performance in waves, the validation of local physical variables is required.

This abstract summarizes the paper of Yang et al. (2021, [1]), which introduces the two computational results and experimental measurement. In this study, the characteristics of wave-induced unsteady pressure, which is one of the primitive physical values in hydrodynamics, on the whole ship surface is studied by a Rankine panel method and a Cartesian-grid method. Global quantities—ship motion responses and added resistance—are validated with experimental data. Then, comparisons between computational results and experimental data have been made for the magnitude of the first-harmonic component of wave-induced pressure on different sections and various vertical locations of the ship.

2 NUMERICAL METHODS

2.1 Rankine Panel Method

A computer program based on a time-domain Rankine panel method, called computer program for linear and nonlinear Wave-Induced loads and SHip motion (WISH), was developed by Seoul National University under the support of several large shipbuilding companies. This program is used for the simulation of nonlinear ship motions in waves and it has been extended and applied to the seakeeping problems for cruise ships and offshore structures, hydro-elasticity analysis such as springing, ship maneuvering, and so on.

To solve the linearized boundary value problem, Green's second identity is applied by discretizing the boundary surface. The Rankine source, which only satisfies the Laplace equation, is distributed to the discretized surface. The velocity potential, wave elevation and normal flux along the fluid boundary were approximated using the B-spline basis function. The first-order pressure about the mean body position can be obtained by Bernoulli's equation and the perturbations of variables with respect to the mean body position, as follows:

$$p^{(1)} = -\rho\left[\left(\frac{\partial}{\partial t} - \mathbf{U}\cdot\nabla\right)(\phi_I + \phi_d) + \nabla\Phi\cdot\nabla(\phi_I + \phi_d) + \boldsymbol{\delta}\cdot\nabla\left(-\mathbf{U}\cdot\nabla\Phi + \frac{1}{2}\nabla\Phi\cdot\nabla\Phi + gz\right)\right] \tag{1}$$

where Φ is the double-body basis potential, subscript I is the component associated with the incident wave, and subscript d is the component associated with the disturbed wave. The linear displacement $\boldsymbol{\delta}$ is defined as $\boldsymbol{\delta}(\mathbf{x},t) = \boldsymbol{\xi}_T(t) + \boldsymbol{\xi}_R(t)\times\mathbf{x}$, and $\boldsymbol{\xi}_T$ and $\boldsymbol{\xi}_R$ indicate linear translational and rotational displacement vectors. The details of numerical implementations of WISH program can be found in Kim and Kim (2011, [3]).

2.2 Cartesian-Grid Method

The wave-ship interaction problem was considered as a multi-phase problem with water, air, and solid phases in the present Cartesian-grid method, called Seoul National University-Marine Hydrodynamics Laboratory-Computational Fluid Dynamics (SNU-MHL-CFD). A solid body was embedded in a Cartesian grid, and to identify the different phases in each grid, the volume-fraction functions were defined for each phase. To capture the free surface, the tangent of hyperbola for interface capturing (THINC) scheme which is one of volume-of-fluid (VOF) methods was used with a weighted line interface calculation (WLIC) method. The volume fraction of a solid body embedded in a Cartesian-grid system was calculated using a level-set algorithm, and the body boundary condition was imposed using a volume-weighted formula. The pressure Poisson equation is solved using a multi-grid algorithm to update the pressure in the fluid domain:

$$\nabla\cdot\left(\frac{1}{\rho}\nabla p\right) = \frac{1}{\Delta t}\nabla\cdot\vec{u} \tag{2}$$

where Δt means the time step. The details of the Cartesian-grid method can be found in Yang et al. (2015, [4]).

3 SIMULATION RESULTS

The RIOS bulk carrier is considered in this study and its body plan and the location of pressure sensors are shown in Fig. 1. The Froude number, Fn = $U/(gL)^{1/2}$ is equal to 0.180 where U is the ship speed, g is the gravitational acceleration, and L is the ship length. The distance between aft perpendicular (AP) and forward perpendicular (FP) is divided into evenly spaced ordinates, which are equal to 0.0 and 10.0 for AP and FP, respectively. In the present comparison, four sections— ordinate (Ord.) = 9.5, 9.0 (near bow), 5.0 (mid-ship), and 0.5 (near stern)—are selected, and the position of pressure measurement in each section is represented as the angle θ from the keel line. That means 0° indicates the keel-line, and 90° indicates the still-water-level, as shown in Fig. 1.

The magnitude of the wave-induced heave, pitch motions, and added resistance of the RIOS bulk carrier is shown in Fig. 2. The numerical computations using the Cartesian-grid method were conducted with $H/\lambda = 1/80$ and 1/40, where H and λ are the wave height and wavelength of the incident wave. In addition, the smaller wave steepness condition ($H/\lambda = 1/125$) was simulated for the cases $\lambda/L = 1.25$. In the experiment (Iwashita et al., 2016 [2]), the wave steepness varied from $H/\lambda = 1/200$ to 1/56. It is difficult to generate the incident wave accurately with small-wave steepness in short-wave cases for both experiment and numerical simulation, while in the Rankine panel method, the linearized free-surface and body boundary conditions were applied. The overall magnitude of heave and pitch motions are similar to each other, whereas for the Cartesian-grid method, smaller heave responses can be found near the resonance region ($\lambda/L = 1.25$). However, if the amplitude of the incident wave decreases, the magnitude of heave motion becomes close to the others. This nonlinearity is known to be responsible for the cross-coupling damping of heave and pitch if the ship has a large flare angle. Both numerical codes provide similar results of added resistance to the experiment in the overall wavelength range. Likewise, in the motion responses, the normalized added resistance decreases as the wave steepness increases in the computational results of the Cartesian-grid method.
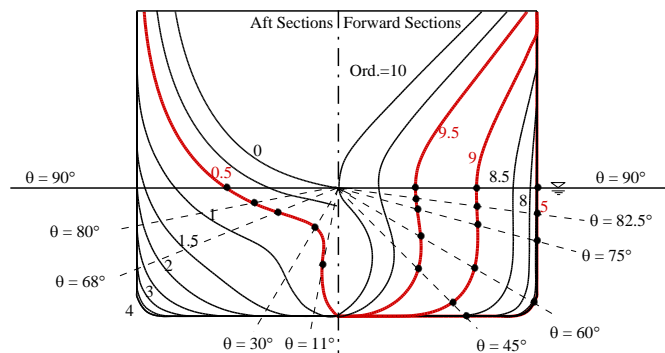

Fig. 1 Body plan and location of pressure sensors of RIOS bulk carrier
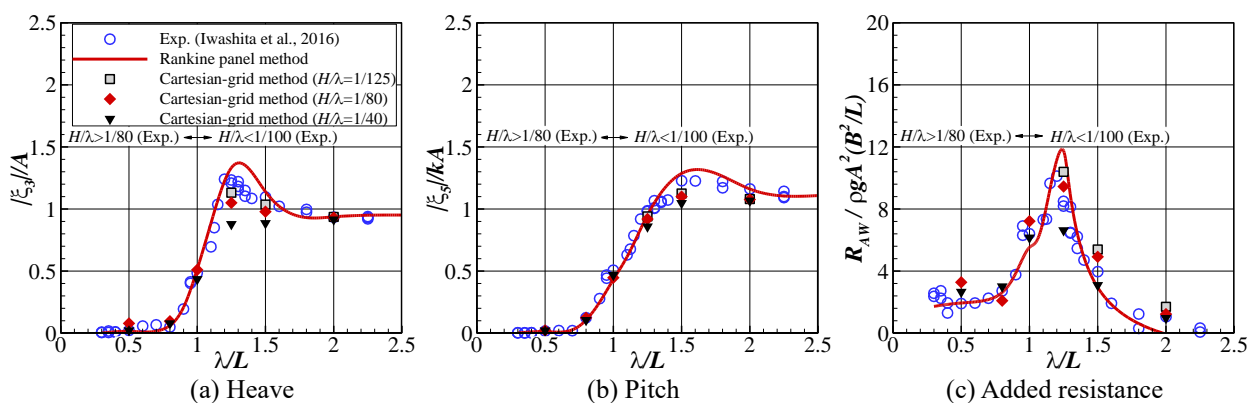

(a) Heave (b) Pitch (c) Added resistance

Fig. 2 Motion amplitude and added resistance of RIOS bulk carrier

The first harmonic amplitudes of the wave-induced pressure distribution over the whole ship surface for two different wavelengths are compared in Fig. 3. The amplitude of the first harmonic from the Rankine panel method near the still-water-level is larger than that from the Cartesian-grid method, especially in the ship bow region, because of the linear assumption. Figure 4 shows the time history of unsteady pressure for Ord. = 9.5. The left column is the resonance case ($\lambda/L = 1.25$), while the right column is the short-wave condition ($\lambda/L = 0.5$). The pressure is normalized with the maximum value of linear dynamic pressure of the incident wave ρgA. The Rankine panel method provides harmonic time series, while the results of the Cartesian-grid method show the half-sine shape for $\theta = 90°$ in the resonance case. This position is

near the still-water-level, and thus the measuring position is regularly exposed to the air, because of large ship motion. On the other hand, the exposed time to the air becomes shorter in the short-wave condition, because the ship motion can be ignored. The pressure time histories at the other positions show similar magnitude and oscillation period between the two numerical computations.

Figure 5 shows the magnitude of the first-harmonic component $p^{(1)}$ for $\lambda/L = 1.25$. The uncertainty of the grid in the Cartesian-grid method is represented as an error bar. The maximum grid uncertainty is less than 5%. The magnitude of the first-harmonic component of wave-induced pressure is higher near the ship bow than for the other parts of the ship, and the maximum value is about four times the maximum value of linear dynamic pressure of the incident wave, because of bow submergence. The first-harmonic component of pressure near the still-water-level from the Cartesian-grid method and experiment is smaller than that of the Rankine panel method, in which the pressure was calculated for the mean body position. The magnitude of the first-harmonic components of the wave-induced pressure gradually decreases to zero above the still-water-level in the results of the Cartesian-grid method.

The first-harmonic component of wave-induced pressure is distributed almost uniformly along the vertical direction in the stern region, and its magnitude is less than or equal to half of the linear dynamic pressure, whereas the value is very small at the mid-ship section. All those results are different from the linear wave theory that the linear dynamic pressure is exponentially decaying in the vertical direction with the factor of kz, where k is the wave number. The discrepancy implies that in these cases, the scattered waves—radiation and/or diffraction waves—are equally important to the incident wave.

(a) $\lambda/L = 0.5$
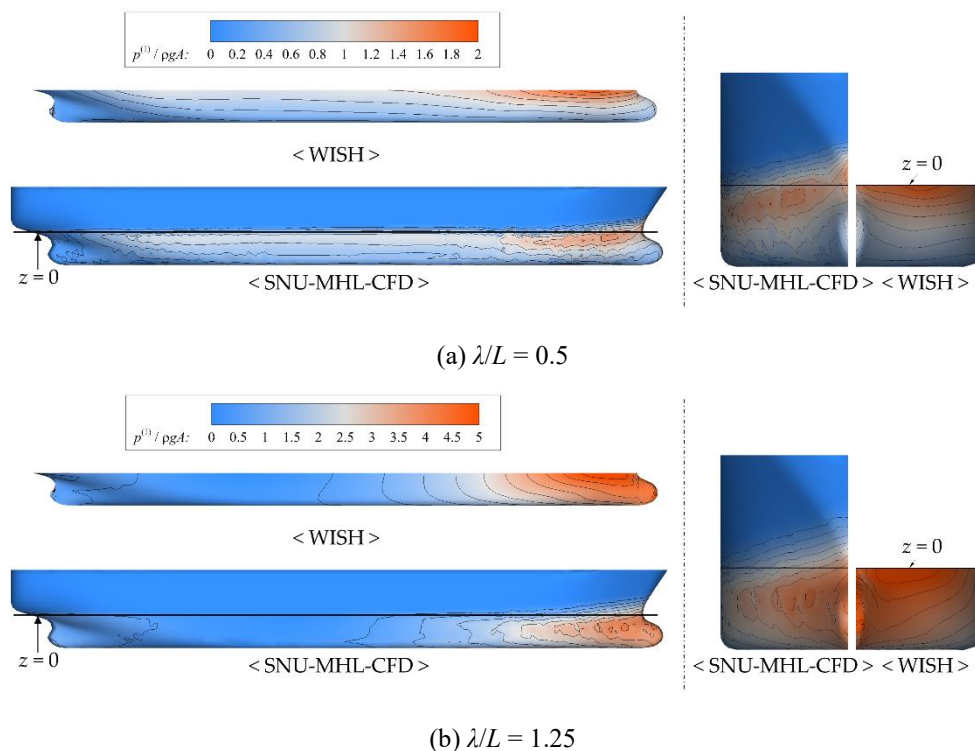

(b) $\lambda/L = 1.25$

Fig. 3 Distribution of the first-harmonic component of dynamic pressure, side view (left) and front view (right) ([1])
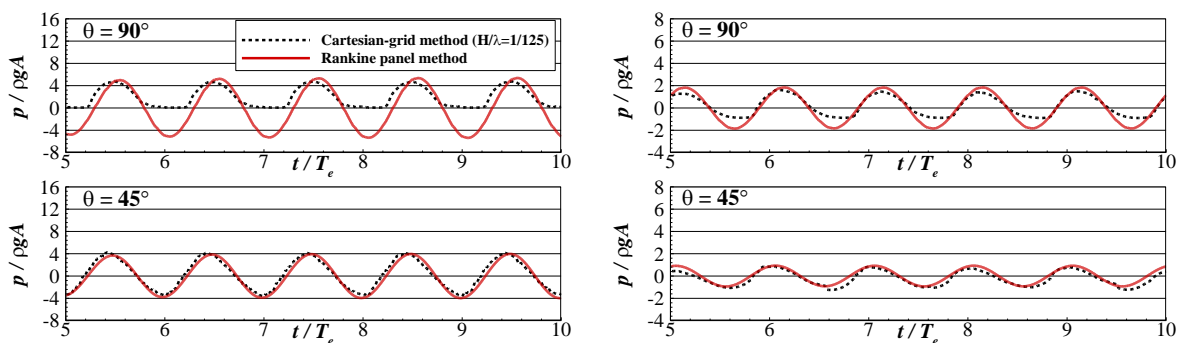

Fig. 4 Time histories of wave-induced pressure, Ord. = 9.5, $\lambda/L = 1.25$ (left) and $\lambda/L = 0.5$ (right) ([1])
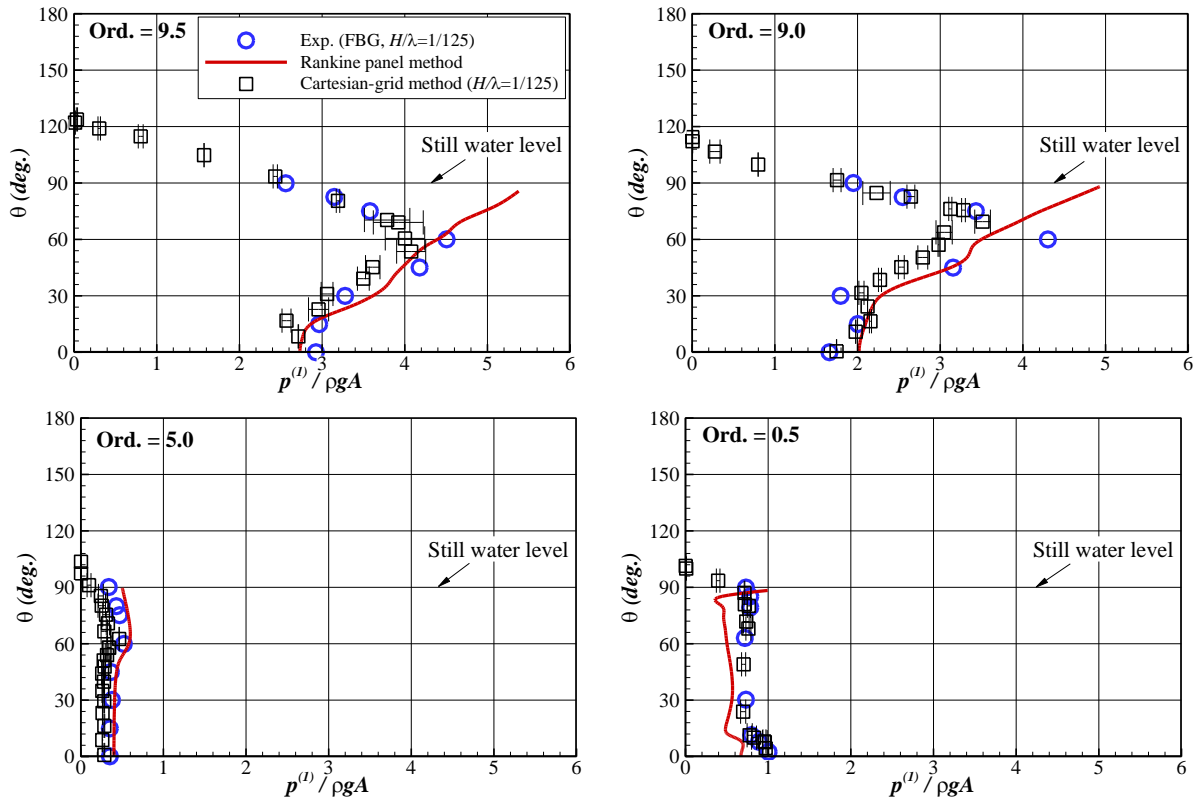
Fig. 5 Magnitude of the first-harmonic pressure component, $\lambda/L = 1.25$

4 CONCLUSION

This study investigated the distribution of unsteady, wave-induced pressure on the ship surface. The results show that the overall accuracy of both numerical methods is acceptable. The nonlinearity of pressure distribution was observed mostly from the pressure near the still-water-level of the ship bow, where the measurement position was regularly exposed to the air. Consequently, the pressure time history near the still-water-level showed half-sine shape, and the first-harmonic component was smaller than that from the Rankine panel method, in which the linearized boundary value problem is solved. The additional computational results will be presented at the workshop.

ACKNOWLEDGEMENTS

REFERENCES

[1] Yang, K.K., Kim, B.S., Kim, Y., Kashiwagi, M., Iwashita, H., 2021. Numerical Study on Unsteady Pressure Distribution on Bulk Carrier in Head Waves with Forward Speed, Processes. (accepted, online available)

[2] Iwashita, H., Kashiwagi, M., Ito, Y., Seki, Y., Yoshida, J., Wakahara, M., 2016. Measurement of unsteady pressure distributions of a ship advancing in waves. In: Proceedings of The Japan Society of Naval Architects and Ocean Engineers, Fukuoka, Japan. (In Japanese)

[3] Kim, K.H., Kim, Y., 2011. Numerical study on added resistance of ships by using a time-domain Rankine panel method. Ocean Eng., 38, 1357–1367.

[4] Yang, K.K., Kim, Y., Nam, B.W., 2015. Cartesian-grid-based computational analysis for added resistance in waves. J. Mar. Sci. Tech., 20, 155–170.